ENVIRONMENTAL RESEARCH
LETTERS

LETTER • OPEN ACCESS

The nonlinear response of fine particulate matter pollution to ammonia emission reductions in North China

To cite this article: Zehui Liu *et al* 2021 *Environ. Res. Lett.* **16** 034014

ENVIRONMENTAL RESEARCH
LETTERS

CrossMark

OPEN ACCESS

RECEIVED
28 October 2020

REVISED
30 December 2020

ACCEPTED FOR PUBLICATION
25 January 2021

PUBLISHED
16 February 2021

LETTER

The nonlinear response of fine particulate matter pollution to ammonia emission reductions in North China

Zehui Liu[1], **Mi Zhou**[1], **Youfan Chen**[1], **Dan Chen**[2], **Yuepeng Pan**[3], **Tao Song**[3], **Dongsheng Ji**[3], **Qi Chen**[4] **and Lin Zhang**[1]

[1] Laboratory for Climate and Ocean-Atmosphere Studies, Department of Atmospheric and Oceanic Sciences, School of Physics, Peking University, Beijing 100871, People's Republic of China
[2] Institute of Urban Meteorology, Beijing 100089, People's Republic of China
[3] State Key Laboratory of Atmospheric Boundary Layer Physics and Atmospheric Chemistry (LAPC), Institute of Atmospheric Physics, Chinese Academy of Sciences, Beijing 100029, People's Republic of China
[4] State Key Joint Laboratory of Environmental Simulation and Pollution Control, BIC-ESAT and IJRC, College of Environmental Sciences and Engineering, Peking University, Beijing 100871, People's Republic of China

E-mail: zhanglg@pku.edu.cn **and** qichenpku@pku.edu.cn

Keywords: ammonia, air pollution, fine particulate matter, $PM_{2.5}$, emission control strategy

Supplementary material for this article is available online

Abstract

Recent Chinese air pollution actions have significantly lowered the levels of fine particulate matter ($PM_{2.5}$) in North China via controlling emissions of sulfur dioxide (SO_2) and nitrogen oxides (NO_x) together with primary aerosols, while the emissions of another precursor, ammonia (NH_3), have not yet been regulated. This raises a question that how effective the NH_3 emission controls can be on the mitigation of $PM_{2.5}$ pollution along with the reduction of SO_2 and NO_x emissions. Here we use a regional air quality model to investigate this issue focusing on the $PM_{2.5}$ pollution in North China for January and July 2015. We find that the efficiency of the $PM_{2.5}$ reduction is highly sensitive to the NH_3 emission and its reduction intensity. Reductions in the population-weighted $PM_{2.5}$ concentration (PWC) in the Beijing–Tianjin–Hebei region are only 1.4–3.8 μg m^{-3} (1.1%–2.9% of $PM_{2.5}$) with 20%–40% NH_3 emission reductions, but could reach 8.1–26.7 μg m^{-3} (6.2%–21%) with 60%–100% NH_3 emission reductions in January 2015. Besides, the 2015–2017 emission changes (mainly reduction in SO_2 emissions) could lower the $PM_{2.5}$ control efficiency driven by the NH_3 reduction by up to 30% for high NH_3 emission conditions, while lead to no change or increase in the efficiency when NH_3 emissions become low. NO_x emission reductions may enhance the wintertime $PM_{2.5}$ pollution due to the weakened titration effect and can be offset by simultaneously controlling NH_3 emissions. Our results emphasize the need to jointly consider NH_3 with SO_2 and NO_x emission controls when designing $PM_{2.5}$ pollution mitigation strategies.

1. Introduction

Fine particulate matter (particle with aerodynamic diameter less than or equal to 2.5 μm; also referred as $PM_{2.5}$) not only poses serious harm to human health but also adversely influences atmospheric environment (Li *et al* 2014, Gao *et al* 2017, Hou *et al* 2019). In recent years, the North China Plain has experienced severe $PM_{2.5}$ air pollution and drawn worldwide attention (Huang *et al* 2014, Zhang *et al* 2015). To abate the $PM_{2.5}$ air pollution, the Chinese government has implemented the 'Action Plan on Prevention and Control of Air Pollution' in 2013 and 'Three-year Action Plan Fighting for a Blue Sky' in 2018 (Chinese State Council 2013, 2018, Zhang *et al* 2019a). As a consequence, the annual mean $PM_{2.5}$ concentration in the Beijing–Tianjin–Hebei (BTH) region has decreased from 106 μg m^{-3} in 2013 to 64 μg m^{-3} in 2017 (MEE 2016, 2018). However, the latter value is still much higher than the China's National Ambient Air Quality Standard of 35 μg m^{-3}, which calls for more stringent emission control measures.

Ammonia (NH_3) is the main alkaline gas in the ambient atmosphere and plays a critical role in nitrogen deposition and haze pollution

(Wang *et al* 2013, Zhang *et al* 2015, Pan *et al* 2018). It first reacts with sulfuric acid (H_2SO_4, typically produced by the oxidation of SO_2) to form ammonium sulfate aerosol, and excessive NH_3 then reacts with nitric acid (HNO_3, produced from the oxidation of NO_2) to form ammonium nitrate aerosol. These secondary inorganic aerosols (SIAs, including sulfate, nitrate, and ammonium) account for 30%–50% of $PM_{2.5}$ in eastern China (Zhao *et al* 2013, Huang *et al* 2014, Sun *et al* 2016). Depending on the abundance of NH_3 in the air, the formation of SIA can be considered as the NH_3-poor condition (when there is insufficient NH_3 to neutralize H_2SO_4) or the NH_3-rich condition (when there is NH_3 to further neutralize HNO_3) (Seinfeld and Pandis 2006). When NH_3 is too excessive, the formation of nitrate becomes HNO_3-limited, and most NH_3 remains gaseous (Xu *et al* 2019). The availability of NH_3 also significantly modulates liquid aerosol pH and then affects the heterogenous production of secondary aerosols (Zheng *et al* 2020).

Clean air actions in China have implemented a series of emission control measures mainly targeting fuel combustion induced emissions of SO_2, NO_x ($NO + NO_2$), and primary aerosols (Zhang *et al* 2019a). Regional NH_3 emissions are dominantly from agricultural activities (i.e. fertilizer application and livestock manure management) (Zhang *et al* 2018) and have not yet been regulated in China (Fu *et al* 2017, Zheng *et al* 2018). The recent 'Three-year Action Plan Fighting for a Blue Sky' called for agricultural NH_3 emission controls but without a specific reduction target (Chinese State Council 2018). Atmospheric chemistry modelling studies indicated that controlling agricultural NH_3 emissions would significantly decrease aerosol nitrate in North China (Han *et al* 2020) in particular during severe winter-haze events (e.g. a decrease of SIA by ∼21% from 40% reduction of the NH_3 emissions in North China found by Xu *et al* (2019)), while thermodynamic calculations suggested that >50% reduction of the NH_3 emissions was required to effectively reduce the SIA levels in this region (Guo *et al* 2018, Song *et al* 2019). The discrepancy can be largely induced by the accuracy of the NH_3-emission estimates. In addition, the effectiveness of NH_3 emission controls on $PM_{2.5}$ along with the rapid changes of the SO_2 and NO_x emissions in North China remains undetermined.

To address these issues, we use a regional air quality model combined with our recent developed Chinese agricultural NH_3 emission inventory (Zhang *et al* 2018). We conduct a series of model simulations to quantify the effectiveness of NH_3 emission controls on the $PM_{2.5}$ pollution under different NH_3 emission reduction conditions as well as under different SO_2 and NO_x emission conditions (e.g. considering the 2015–2017 SO_2/NO_x emission changes).

Table 1. Emission settings in the WRF-Chem simulation scenarios.

Simulation scenario	Description
Base	The 2015 emission conditions, also referred as S1R0
S1R*N* ($N = 20/40/60/100$)	NH_3 emission is reduced by 20%, 40%, 60%, 80% and 100%, respectively.
S2R*N* ($N = 0/20/40/60/100$)	Similar to S1R*N*, but further reduces the NO_x and SO_2 emissions from the levels of 2015 to those of 2017 in North China.
S3R*N* ($N = 0/20/40/60/100$)	Similar to S2R*N*, but further reduces NO_x emissions by 20% in North China.

2. Methodology and data

2.1. The WRF-Chem model

The Weather Research and Forecasting (WRF) version 3.6.1 model coupled with Chemistry (WRF-Chem) is employed to simulate the meteorology and atmospheric chemistry. The modeling framework is configured with two domains (figure S1 (available online at stacks.iop.org/ERL/16/034014/mmedia)) using 161 (east–west) × 171 (south–north) and 150 (east–west) × 159 (south–north) grid cells at 27 km and 9 km horizontal resolutions, respectively. The outer domain covers China and its adjacent areas, and the inner domain covers North China (110°–120° E and 35°–43° N; figure S1) where this study focuses on. The National Center for Environmental Prediction Final (FNL) Analysis data with 1° spatial resolution and 6 h temporal resolution are used for the initial and lateral meteorological boundary conditions. The meteorological fields are re-initiated every 2 d using the FNL Analysis data to prevent the simulated meteorology drifting away from the actual conditions, so that they are nearly the same for all our simulation scenarios (table 1) with slight differences likely driven by the coupling of chemistry and meteorology. The chemical initial and boundary conditions are from the outputs of the global chemical transport model MOZART-4 (Emmons *et al* 2010).

Our simulations use the gas-phase Carbon-Bond Mechanism Z mechanism (Zaveri and Peters 1999) coupled with a four-bin sectional (with dry diameters of 0.039–0.156, 0.156–0.625, 0.625–2.5, and 2.5–10.0 μm) Model for Simulating Aerosol Interactions and Chemistry aerosol scheme (Zaveri *et al* 2008). Formation of sulfate aerosol in the model accounts for gas-phase oxidation SO_2, and aqueous-phase oxidation of SO_2 by H_2O_2 and O_3 in clouds. We include the heterogeneous sulfate formation reactions on particle surface based on Chen *et al* (2016) to improve the

model simulation of SIA. The NH_3 and HNO_3 gas-aerosol equilibrium is determined by the gas-particle partitioning module Adaptive Step Time-Split Euler Method (Zaveri *et al* 2008). We increase the anthropogenic organic carbon (OC) emissions by a factor of 4 in July to account for secondary organic aerosols in the model (Sun *et al* 2012) as our model configuration does not consider online secondary organic aerosols (SOA) formation. This SOA assumption shall not affect our analyses because the chemistry of SIA and SOA is uncoupled in the model.

The model physical settings include the Morrison double-moment microphysics scheme (Morrison *et al* 2009), the Grell-3 cumulus scheme (Grell *et al* 2002), the Rapid Radiative Transfer Model long-wave radiation scheme (Mlawer *et al* 1997), the Goddard short-wave radiation scheme (Chou *et al* 1994), the Yonsei University planetary boundary layer scheme (Hong *et al* 2006), the revised MM5 (fifth-generation Mesoscale Model) Monin–Obukhov surface layer scheme, and the Unified Noah land-surface model (Chen and Dudhia 2001). A single-layer Urban Canopy Model is used to explicitly simulate the urban areas (Kusaka *et al* 2001). We have further updated the land use types with the 2015 Moderate Resolution Imaging Spectroradiometer Land Cover Type (MCD12Q1) Version 6 data product (https://lpdaac.usgs.gov/products/mcd12q1v006/).

Anthropogenic emissions are from the 2015 Multi-resolution Emission Inventory for China (MEIC, www.meicmodel.org/) and the 2010 MIX inventory for regions outside mainland China (Li *et al* 2017), except for Chinese agricultural NH_3 emissions that are from Zhang *et al* (2018) with updated statistics for the year 2015. Biogenic emissions are calculated online using the Model of Emissions of Gases and Aerosols from Nature (Guenther *et al* 2006). Biomass burning emissions are from the Fire Inventory from the NCAR (Wiedinmyer *et al* 2011). Figure S2 shows the spatial distributions of NH_3, SO_2, and NO_x emissions over North China in January and July 2015, and table S1 summarizes the emission totals. Our estimates of anthropogenic NH_3 emissions in North China are 0.11 Tg month^{-1} in January and 0.25 Tg month^{-1} in July. Compared with the MEIC NH_3 emissions, our estimates are about 1% lower in January and 44% higher in July. Our study does not consider bi-directional NH_3 fluxes (Bash *et al* 2013), and treats emission and deposition as separate processes. This may affect model SIA simulation (Zhu *et al* 2015), and needs to be evaluated in future work.

We conduct a series of WRF-Chem simulations as summarized in table 1. First, the baseline simulation (Base, also denoted as the S1R0 scenario) includes the emissions described above and can be evaluated with observations. Second, a group of sensitivity simulations (S1R*N*) by reducing anthropogenic NH_3 emissions over North China by 20%, 40%, 60%, 80%, and 100%, respectively (denoted as S1R*N* scenarios, $N = 20/40/60/100$). The differences in $PM_{2.5}$ concentrations between S1R0 and S1R*N* then estimate the effects of NH_3 emission reductions. Third, a group of sensitivity simulations (S2R*N*, $N = 0/20/40/60/100$), similar to S1R*N*, but reduces anthropogenic SO_2 emissions by ~40% and anthropogenic NO_x emissions by ~8% in North China to reflect emission changes from 2015 to 2017 (Zheng *et al* 2018; figure S3). Fourth, another group of sensitivity simulations, similar to S2R*N*, but further reduces anthropogenic NO_x emissions in North China by 20% (S3R*N*, $N = 0/20/40/60/100$) reflecting potential NO_x emissions reduction in the next few years (Liu *et al* 2016). For all simulations, a winter month (January) and a summer month (July) in 2015 are simulated after 3 d spin-up for initialization. We find a longer spin-up time of 10 d only slightly change the model simulations.

2.2. Meteorology and surface measurements

For model evaluation, meteorological observations including 10 m wind direction (WD10), 10 m wind speed (WS10), 2 m air temperature (T2), and 2 m relative humidity (RH2) in January and July 2015 at 36 stations in North China are collected from National Climatic Data Center (https://ncdc.noaa.gov/isd/data-access). Hourly observations of surface $PM_{2.5}$ concentrations at 39 stations in North China are obtained from the Ministry of Ecology and Environment of China (http://106.37.208.233:2035/).

Monthly NH_3 concentrations at seven sites from the Ammonia Monitoring Network in China (AMoN-China; Pan *et al* 2018) are used to evaluate our NH_3 emission inventory in North China. We use NH_3 measurements from AMoN-China conducted during 01–31 January and 15–31 July 2015. We use measurements of $PM_{2.5}$ components, including sulfate (SO_4^{2-}), nitrate (NO_3^-), ammonium (NH_4^+), OC, and black carbon in January and July 2015 at Beijing (39.94° N, 116.38° E) and Tianjin (39.09° N, 117.31° E) obtained by the Institute of Atmospheric Physics. Hourly model results are sampled at the grids covering the stations. Correlation coefficient (R) and mean bias (MB) between observations and model results are calculated.

3. Results

3.1. Observed and simulated surface pollutant concentrations

Evaluations of model simulated meteorological variables (WD10, WS10, T2, and RH2) are shown in figure S4. The spatial patterns of simulated meteorological variables are overall in good agreement with observations in North China. Figure 1 shows the time series and spatial distributions of observed and base-simulated $PM_{2.5}$ concentrations over North China in January (figures 1(a) and (b)) and July

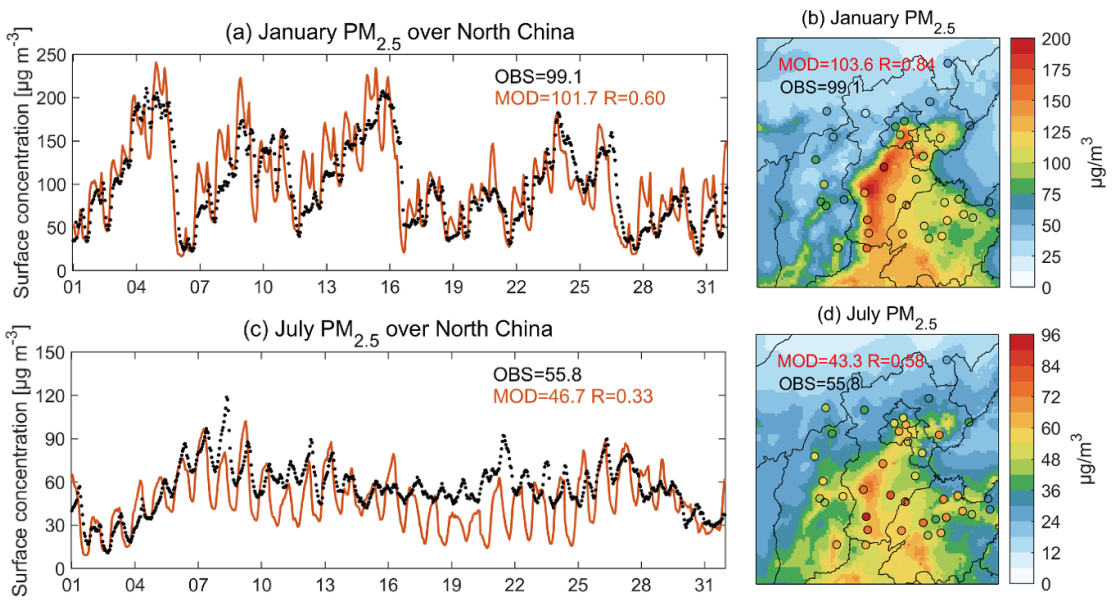

Figure 1. Observed and WRF-Chem base simulated surface $PM_{2.5}$ concentrations over North China in January and July 2015. The left panels show time series of hourly observations (black dots) and model results (red lines) by averaging 39 stations in North China. The right panels show spatial distributions of observed (circles) and simulated (contours) monthly mean concentrations. Mean observed values (OBS) and corresponding model results (MOD), and their correlation coefficients (temporally and spatially) are shown inset.

(figures 1(c) and (d)) 2015. The comparisons of $PM_{2.5}$ components with measurements at Beijing and Tianjin are shown in figure S5. The WRF-Chem base simulation in general captures the magnitudes and variations of observed surface $PM_{2.5}$ concentrations in both January and July with R values of >0.60 in January and >0.33 in July. The MB is small (2.6 μg m^{-3}) in January and relatively large in July (−9.1 μg m^{-3}). Evaluations with measurements of $PM_{2.5}$ components show that the model simulated SIA concentrations are biased low by 10%–40% in July, especially for sulfate. The reasons why our model biases are larger in July than January are unclear, and may reflect uncertainties in emissions and aerosol processes. The implemented heterogeneous sulfate formation herein (Chen *et al* 2016) perhaps needs further enhancements in summer. Model simulated RH2 fields over North China also show larger negative biases in July than January (figure S4).

We compare in figure 2 the spatial distributions of the measured and simulated surface NH_3 concentrations over North China for 01–31 January (figure 2(a)) and 15–31 July (figure 2(b)) 2015. Although the measured and base-simulated NH_3 concentrations show similar spatial variations (R values of 0.93 in January and 0.72 in July), the base-model results are biased high by 38% (simulated 11.6 μg m^{-3} vs observed 8.4 μg m^{-3}) in January and biased low by 30% (15.2 μg m^{-3} vs 21.5 μg m^{-3}) in July. We find that when we decrease/increase anthropogenic NH_3 emissions by 20% in January/July, the biases can be corrected in January/reduced to only −12% in July (figures 2(c) and (d)). This indicates that our base NH_3 emissions might be overestimated in January while underestimated in July over North China. Such a strong seasonality in NH_3 emissions was also previously found by Zhang *et al* (2019b). Comparisons of simulated NH_3 columns with the Infrared Atmospheric Sounding Interferometer (IASI) satellite observations (Van Damme *et al* 2014) over China also support the spatial distributions of NH_3 emissions and indicate similar model biases in the 2 months to those inferred by the surface measurements (figure S6).

To further illustrate the effect of NH_3 emission changes on surface concentrations, we show in figures 2(e) and (f) changes in BTH regional mean gaseous NH_3, aerosol NH_4^+, and total reduced nitrogen ($NH_x = NH_3 + NH_4^+$) as we gradually reduce anthropogenic NH_3 emissions in North China (i.e. S1R*N* scenarios). When we begin to decrease NH_3 emissions (reductions <40%), surface NH_3 concentrations decrease rapidly while NH_4^+ concentrations decrease much slower, reflecting NH_3-excessive conditions with current emissions. However, under large emission reductions (>60%), changes in NH_4^+ concentrations become faster than NH_3 concentrations. The different responses of gaseous NH_3 and aerosol NH_4^+ to emission reductions suggest changes in their partitioning and thus the lifetime of NH_x as gaseous NH_3 has a shorter lifetime than aerosol NH_4^+. Regionally, the changes balance each other, leading a close-to-linear response of NH_x concentrations to NH_3 emission reductions for both months. This is consistent with previous studies that suggest atmospheric NH_x is a better indicator of NH_3 emissions than NH_3 or NH_4^+ alone in the US (Pinder *et al* 2006, Zhang *et al* 2012).

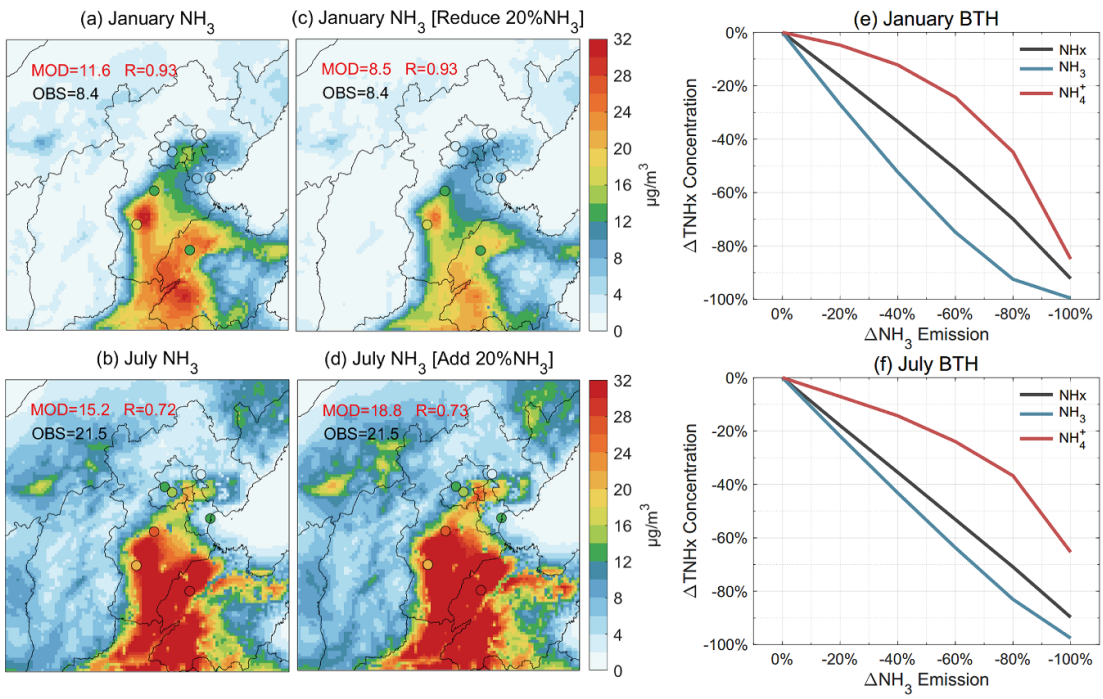

Figure 2. Observed and simulated surface NH_3 concentrations in North China for the periods of 01–31 January (top panels) and 15–31 July (bottom panels) 2015. The left panels show comparison of measurements (circles) with the base simulation, and central panels show comparisons with sensitivity simulations (with NH_3 emissions in North China reduced by 20% for January and increased by 20% for July). Regional mean observed values (OBS) and corresponding model results (MOD), and their correlation coefficients are shown inset. The right panels show changes in Beijing–Tianjin–Hebei (BTH) mean gaseous NH_3 (blue lines), aerosol ammonium (NH_4^+, red lines), and total reduced nitrogen ($NH_x = NH_3 + NH_4^+$, black lines) when NH_3 emissions in North China are decreased for January and July 2015.

3.2. Response of $PM_{2.5}$ pollution to NH_3 emission reductions

The sensitivity simulations with perturbed NH_3 emissions allow us to assess the responses of air pollution to NH_3 emission reductions. Figure 3 shows changes in surface $PM_{2.5}$ concentrations as we gradually reducing NH_3 emissions in North China in January 2015. To describe the saturation of atmospheric NH_3, we follow previous studies (Song *et al* 2018, Xu *et al* 2019) and define the excess NH_3 (in unit of $\mu g\ m^{-3}$) as the differences in NH_x and required NH_3 to meet ionic equilibrium using the formula below:

$$\text{Excess NH}_3 = \text{Total NH}x - \text{required NH}_3. \quad (1)$$

$$\text{Total NH}x = 17 \times \left(\frac{[NH_4^+]}{18} + \frac{[NH_3]}{22.4} \right). \quad (2)$$

$$\text{Required NH}_3 = 17 \times \left(\frac{[SO_4^{2-}]}{48} + \frac{[NO_3^-]}{62} + \frac{[Cl^-]}{35.5} + \frac{[HNO_3]}{22.4} + \frac{[HCl]}{22.4} - \frac{[Na^+]}{23} \right) \quad (3)$$

where $[NH_4^+]$, $[SO_4^{2-}]$, $[NO_3^-]$, $[Cl^-]$, and $[Na^+]$ are the mass concentrations (in unit of $\mu g\ m^{-3}$) of these ions, and $[NH_3]$, $[HNO_3]$, and $[HCl]$ are gas mixing ratios (ppb) converting to molar unit with the value of 22.4 L mol^{-1} at the standard atmospheric condition.

As shown in figure 3, changes of mean $PM_{2.5}$ concentration in January become much more distinct with stronger NH_3 emission reductions in the region. The first 20% NH_3 emission reduction would only decrease $PM_{2.5}$ in Beijing by 1.6 $\mu g\ m^{-3}$ and by 1.4 $\mu g\ m^{-3}$ in BTH. The values increase to 8.3 $\mu g\ m^{-3}$ in Beijing and 7.0 $\mu g\ m^{-3}$ in BTH with 60% NH_3 emission reductions, and 20.8 $\mu g\ m^{-3}$ in Beijing and 20.4 $\mu g\ m^{-3}$ in BTH when all NH_3 emissions are turned off. The largest $PM_{2.5}$ responses shift towards the southern Hebei province where $PM_{2.5}$ concentrations are particularly high (figure 1(a)). Such nonlinear responses can be largely explained by the derived excess NH_3 in each scenario. As also shown in figure 3, NH_3 is highly saturated in the southern Hebei province in the base condition and scenarios with small NH_3 emission reductions, and thus the SIA portion of $PM_{2.5}$ are insensitive to NH_3 emissions. We find similar results for July but with smaller $PM_{2.5}$ decreases under strong NH_3 emission reductions than those in January (figure S7).

Figure 4 summarizes the changes of mean concentrations of $PM_{2.5}$ and its components in BTH as driven by NH_3 emission changes in North China for January and July 2015. The decreases of $PM_{2.5}$ concentration associated with NH_3 emission reductions

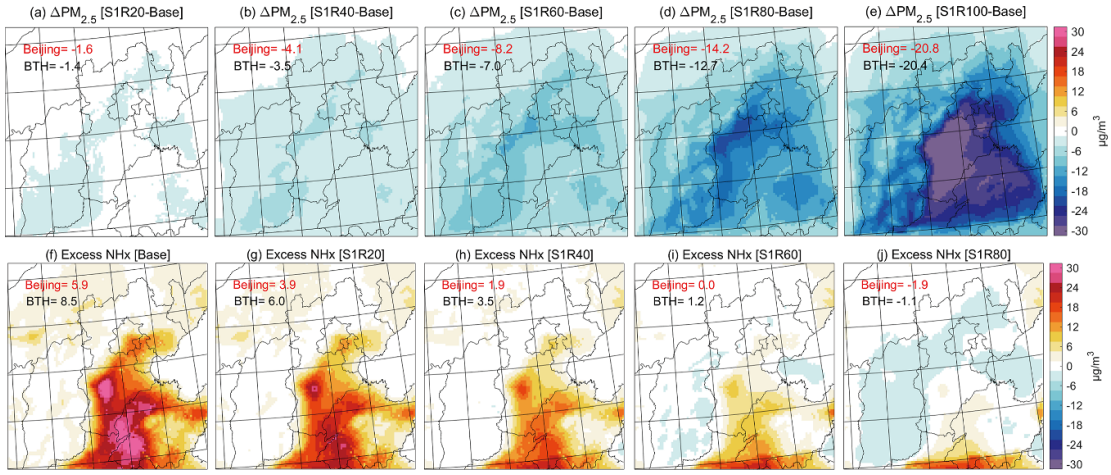

Figure 3. (Top panels) January mean changes in surface $PM_{2.5}$ concentrations due to NH_3 emission reductions in North China estimated as the differences between the base simulation and S1R*N* scenarios with NH_3 emissions reduced by *N*% ($N = 20/40/60/80/100$). (Bottom panels) Excess NH_3 concentrations in January as estimated by the formula described in the text for the base simulation and S1R*N* scenarios ($N = 20/40/60/80$). Regional mean values in Beijing and in BTH are shown inset.

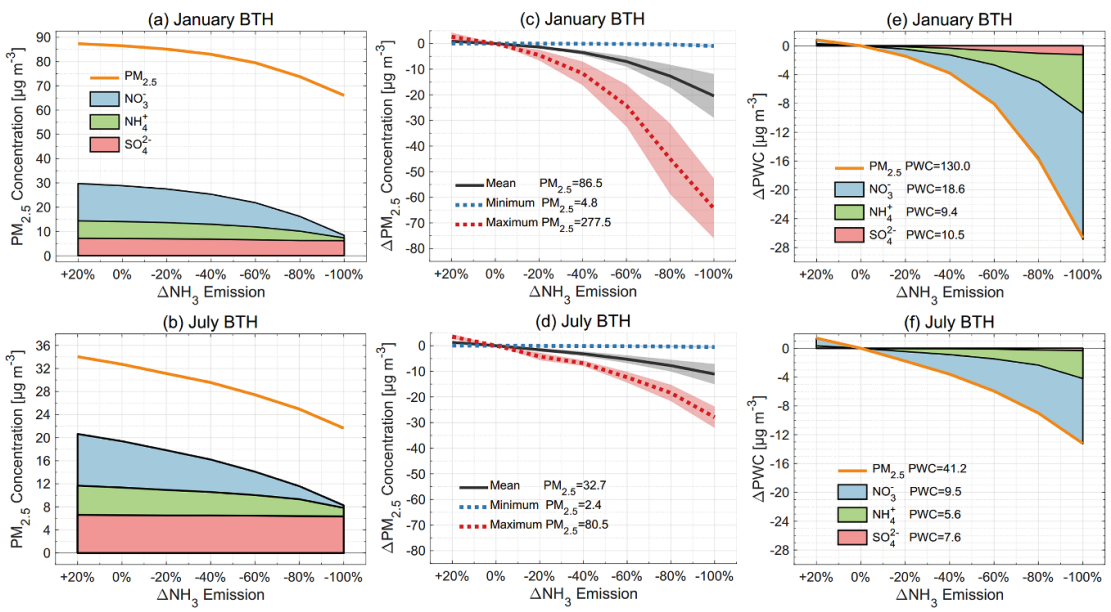

Figure 4. Effectiveness of NH_3 emission reductions in North China on BTH regional mean surface $PM_{2.5}$ pollution in January (top panels) and July (bottom panels) 2015. The left panels show BTH geometric mean $PM_{2.5}$ (orange lines), sulfate (red shading), ammonium (green shading), and nitrate (blue shading) levels. The central panels show reductions in monthly mean (black lines), minimum (blue dashed lines), and maximum (red dashed lines) $PM_{2.5}$ concentrations. The right panels show changes in population-weighted $PM_{2.5}$ concentration (PWC) together with sulfate, ammonium, and nitrate contributions. Numbers inset are their values ($\mu g\ m^{-3}$) in the base simulation.

follow a power exponential function in January leading to small $PM_{2.5}$ changes with small NH_3 emission reductions. The responses in July are closer to a linear function, reflecting a stronger sensitivity to NH_3 due to greater HNO_3 availability in summer than in winter. The mean BTH $PM_{2.5}$ in July would be decreased by 1.6/5.3/11.1 $\mu g\ m^{-3}$ with 20%/60%/100% NH_3 emission reductions in North China. The $PM_{2.5}$ components in both months show that sulfate has minor changes but nitrate can be substantially decreased with reducing NH_3 emissions, as also found by Han *et al* (2020). The small decreases in sulfate concentrations under strong NH_3 emission reductions in January are caused by slightly lower sulfate formation on aerosol surface under these scenarios in the model. We find stronger $PM_{2.5}$ responses in heavy pollution episodes in both months. As shown in figure 4, for the heavy pollution episodes, defined as the highest 5% $PM_{2.5}$ concentrations, their values can be decreased by 4.5/24.2/64.4 $\mu g\ m^{-3}$ when NH_3 emissions in North China are reduced by 20%/60%/100% in January. By contrast, the cleanest 5% $PM_{2.5}$ concentrations have insignificant change associated with NH_3 emission reductions.

Figure 4 also shows the responses of $PM_{2.5}$ PWC in North China as a metric more relevant to human health using population data from the Gridded Population of the World version 4 (GPWv4) dataset (CIESIN 2018). PWC values show similar but larger responses than the regional geometric means. When NH_3 emissions in North China are reduced by 20%–40%, monthly mean BTH PWC could be reduced by 1.4–3.8 μg m^{-3} (1.1%–2.9% of PWC) in January and 1.8–3.6 μg m^{-3} (4.3%–8.7% of PWC) in July. When NH_3 emissions are reduced by 60%–100%, BTH PWC would be reduced by 8.1–26.7 μg m^{-3} (6.2%–21% of PWC) in January and 5.9–13 μg m^{-3} (14%–32% of PWC) in July, illustrating $PM_{2.5}$ air quality improvements we can achieve by the NH_3 emission controls under the 2015 emission condition.

The analyses above have emphasized strong nonlinear responses of $PM_{2.5}$ concentrations to NH_3 emission changes in North China. To better quantify their effectiveness, we further calculate the efficiency of NH_3 emission controls based on the sensitivity simulations as $\beta_1 = \frac{\Delta \mathrm{PWC}}{\mathrm{PWC}} / \frac{\Delta E}{E}$, where $\frac{\Delta \mathrm{PWC}}{\mathrm{PWC}}$ is the relative change of PWC and $\frac{\Delta E}{E}$ is the relative change of NH_3 emissions in North China, denoting the relative response of PWC in percentage to 1% reduction in NH_3 emissions under each NH_3 emission scenario. We also calculate the absolute efficiency $\beta_2 = \Delta \mathrm{PWC}/\Delta E$,, describing changes in $PM_{2.5}$ per unit mass change in NH_3 emissions as shown in figure S8. We find for the 2015 emission condition, the BTH mean β_1 efficiencies in January increase from 0.055%/% in the base condition to 0.48%/% (a factor of 8.7 higher) when NH_3 emissions are reduced by 80%. The β_1 efficiencies in July also indicate a nonlinear response, yet much weaker than January, with values of 0.22%/% for the base condition and 200% higher (0.65%/%) when NH_3 emissions are 80% lower.

The effect of NH_3 emission reduction on $PM_{2.5}$ air pollution is thus highly sensitive to its emission estimate. A lower NH_3 emission estimate over North China would present a higher efficiency of NH_3 emission controls for mitigating $PM_{2.5}$ air pollution in this region. Xu *et al* (2019) reported a 40% decrease in aerosol nitrate with NH_3 emissions over North China reduced by 40% in winter. This efficiency is higher than our estimate, which may be attributed to a lower wintertime NH_3 emission (Kang *et al* 2016) in their study (figure S2). Future work is required to accurately constrain the NH_3 emissions.

3.3. Effects of NO_x and SO_2 emission changes

We now quantify the influence of NO_x and SO_2 emission reductions on the efficiency of NH_3 emission controls. This can be estimated by comparing the S1R*N* with S2R*N* and S3R*N* scenarios. As described above, S1R*N* scenarios reflect NH_3 emission reductions for the 2015 emission condition, S2R*N* scenarios reflect the 2017 condition, and S3R*N* scenarios further consider 20% NO_x emission reduction. The differences of S2R0 minus Base and S3R0 minus S2R0 then estimate, respectively, the impacts of 2015–2017 SO_2/NO_x emission changes and 20% further NO_x emission reductions. The 2015–2017 emission changes have led to decreases in BTH $PM_{2.5}$ in both months, mainly driven by the SO_2 emission reductions (figure S9), while with further 20% NO_x emission reductions the BTH regional mean $PM_{2.5}$ would increase by 1.0 μg m^{-3} in January (figure S9). Reducing North China NO_x emissions alone in winter would increase ozone levels due to weakened titration and further enhance the formation of secondary aerosols, as recently found during the COVID-19 pandemic (Huang *et al* 2020).

Figure 5 shows the changes in BTH PWC and β_1 efficiency of NH_3 emission reduction in the S1R*N*, S2R*N*, and S3R*N* scenarios for January and July 2015. We notice that the effects of 2015–2017 SO_2/NO_x emission reductions (i.e. ~40% reduction in SO_2 emissions and ~8% reduction in NO_x emissions) on BTH PWC improvements (4.6 μg m^{-3} in January and 4.9 μg m^{-3} in July) are comparable to 40%–60% NH_3 emission reduction in 2015. The maximum BTH PWC reductions as can be achieved by NH_3 emission controls are 26.7 μg m^{-3} in January and 13.2 μg m^{-3} in July for the S1R*N* scenarios, and 27.6 μg m^{-3} in January and 9.4 μg m^{-3} in July for the S3R*N* scenarios. The much larger differences between S1R*N* and S3R*N* in July (13.2 vs 9.4 μg m^{-3}) than January (26.7 vs 27.6 μg m^{-3}) are mainly driven by the different responses of $PM_{2.5}$ to the 20% NO_x emission reduction. We can see that the impacts of the further 20% NO_x emission reduction on BTH PWC (as contributed by decreases in nitrate) in July become smaller with lower NH_3 emissions.

Changes in SO_2 and NO_x emissions can thus affect the efficiency of NH_3 emission reduction on $PM_{2.5}$ pollution. The 2015–2017 emission changes have generally decreased β_1 efficiencies (figure 5), for no NH_3 emission reduction scenarios, from 0.055%/% to 0.038%/% (30% reduction) in January and from 0.22%/% to 0.19%/% (14% reduction) in July. SO_2 emission controls, in one way, decrease the formation of ammonium sulfate aerosol, causing NH_3 in the air being more saturated, and in another way, enhance the formation of nitrate aerosol when more gaseous NH_3 is available. The net effects as can be seen in figure 5 are decreases in the efficiency under high NH_3 emission conditions, and no change or increase for low NH_3 emission conditions. The additional 20% NO_x emission reduction would further suppress β_1 efficiencies in July by decreasing HNO_3 availability but increase them in January, reflecting the enhanced nitrate formation due to NO_x emission reduction in BTH winter as discussed above. Our results indicate that starting NH_3 emission controls at a stage with high SO_2/NO_x emissions will be more effective for $PM_{2.5}$ air pollution regulation, and a joint

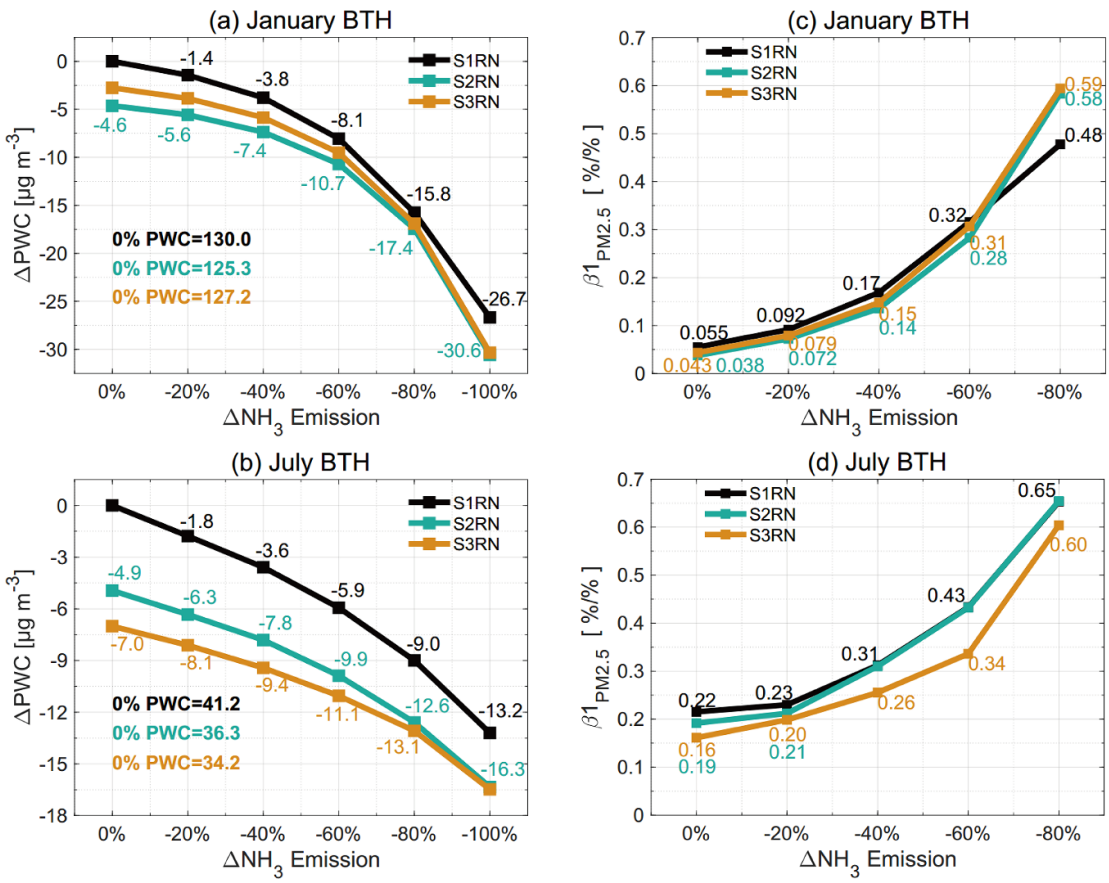

Figure 5. Changes in BTH PWC (left panels) and NH_3 emission reduction efficiency (right panels) in the S1R*N* scenarios (black lines; the 2015 emission condition), S2R*N* scenarios (green lines; the 2017 emission condition), and S3R*N* scenarios (orange lines, the 2017 emission condition with NO_x emission further reduced by 20%) in January (top panels) and July (bottom panels). BTH PWC changes are relative to the base-simulated results (i.e. S1R0). PWC values for S1R0, S2R0, and S3R0 are given inset.

NO_x and NH_3 emission control in winter will be more effective than controlling NO_x alone.

4. Conclusions

In summary, we have shown strong nonlinear responses of the $PM_{2.5}$ air pollution to NH_3 emission controls in North China. Using three sets of model simulations testing NH_3 emission reductions under different SO_2/NO_x emission conditions, we find that under the current emission condition, changes in the $PM_{2.5}$ concentration in North China associated with NH_3 emission reductions follow a power exponential function in January. The BTH PWC in January would only decrease by 1.4–3.8 $\mu g\ m^{-3}$ (1.1%–2.9% of $PM_{2.5}$) when NH_3 emissions in North China were reduced by 20%–40%, but the decreases would reach 8.1–26.7 $\mu g\ m^{-3}$ (6.2%–21% of $PM_{2.5}$) with 60%–100% NH_3 emission reductions. Such nonlinearity reflects a switch of NH_3-excessive to NH_3-limited conditions for SIA, in particular, nitrate formation. The $PM_{2.5}$ changes in July also show a nonlinear response, but the nonlinearity is much weaker than in January.

As SO_2 emissions in North China have substantially reduced over 2015–2017, we find that has lowered the efficiency of NH_3 emission controls on the $PM_{2.5}$ air pollution in both winter and summer by up to 30% for high NH_3 emission conditions, but lead to no change or increase in the efficiency when NH_3 emissions are low. Future reduction of NO_x emissions may partly enhance the $PM_{2.5}$ pollution in BTH winter due to the weakened titration effect, and can be offset by jointly controlling NH_3 emissions.

The Chinese government has implemented a series of active clean air actions in recent years (Zheng *et al* 2018, Zhang *et al* 2019a). China's anthropogenic emissions were estimated to decrease by 62% for SO_2 and 17% for NO_x over 2010–2017, while NH_3 emissions slightly increased by 1% due to the absence of NH_3 emission controls (Zheng *et al* 2018). In the next 5–10 years, changes in SO_2 emissions might level off as the power plants have operated with ultralow emission standards, while NO_x emissions will become stringently controlled to ensure further air quality improvements (Zheng *et al* 2018). Such future SO_2/NO_x emission changes would increase the efficiency of NH_3 emission controls in winter. Our results emphasize the need to jointly consider emission reductions of SO_2, NO_x, and NH_3 for mitigating SIA air pollution. In addition to the air quality effect, NH_3 emission controls can also lead to

other environmental benefits, such as reducing nitrogen deposition and water pollution (Guo *et al* 2020), which should be considered in current environmental strategies.

Data availability statement

The data that support the findings of this study are available upon reasonable request from the authors.

Acknowledgments

This work is supported by the National Key Research and Development Program of China (2018YFC0213304), the National Natural Science Foundation of China (NSFC, 41922037, 41875165), and the Beijing Municipal Science and Technology Project (Z181100005418016). The work also contributes to UNCNET, a project funded under the JPI Urban Europe/China collaboration, Project Numbers 71961137011 (NSFC, China), UMO-2018/29/Z/ST10/02986 (NCN, Poland), and 870234 (FFG, Austria).

ORCID iDs

Zehui Liu https://orcid.org/0000-0001-9967-4344
Lin Zhang https://orcid.org/0000-0003-2383-8431

References

Bash J O *et al* 2013 Evaluation of a regional air-quality model with bidirectional NH_3 exchange coupled to an agroecosystem model *Biogeosciences* **10** 1635–45

Center for International Earth Science Information Network (CIESIN) Columbia University 2018 Gridded Population of the World, Version 4 (GPWv4): Population Count, Revision 11 (Palisades, NY: NASA Socioeconomic Data and Applications Center (SEDAC)) (https://doi.org/10.7927/H4JW8BX5) (Accessed: 30 January 2021)

Chen D *et al* 2016 Simulations of sulfate–nitrate–ammonium (SNA) aerosols during the extreme haze events over northern China in October 2014 *Atmos. Chem. Phys.* **16** 10707–24

Chen F and Dudhia J 2001 Coupling an advanced land surface–hydrology model with the Penn State–NCAR MM5 modeling system. Part I: model implementation and sensitivity *Mon. Weather Rev.* **129** 569–85

Chou M D *et al* 1994 An efficient thermal infrared radiation parameterization for use in general circulations models *NASA Tech. Memo.* No. 104606 (Washington, DC: NASA) (https://ntrs.nasa.gov/api/citations/19950009331/downloads/19950009331.pdf)

Emmons L K *et al* 2010 Description and evaluation of the model for ozone and related chemical tracers, version 4 (MOZART-4) *Geosci. Model Dev.* **3** 43–67

Fu X *et al* 2017 Increasing ammonia concentrations reduce the effectiveness of particle pollution control achieved via SO_2 and NO_X emissions reduction in East China *Environ. Sci. Technol. Lett.* **4** 221–7

Gao J *et al* 2017 Haze, public health and mitigation measures in China: a review of the current evidence for further policy response *Sci. Total Environ.* **578** 148–57

Grell G A *et al* 2002 A generalized approach to parameterizing convection combining ensemble and data assimilation techniques *Geophys. Res. Lett.* **29** 38-1–4

Guenther A *et al* 2006 Estimates of global terrestrial isoprene emissions using MEGAN (Model of Emissions of Gases and Aerosols from Nature) *Atmos. Chem. Phys.* **6** 3181–210

Guo H *et al* 2018 Effectiveness of ammonia reduction on control of fine particle nitrate *Atmos. Chem. Phys.* **18** 12241–56

Guo Y *et al* 2020 Air quality, nitrogen use efficiency and food security in China are improved by cost-effective agricultural nitrogen management *Nat. Food* **1** 648–58

Han X *et al* 2020 Numerical analysis of agricultural emissions impacts on PM2.5 in China using a high-resolution ammonia emission inventory *Atmos. Chem. Phys.* **20** 9979–96

Hong S-Y *et al* 2006 A new vertical diffusion package with an explicit treatment of entrainment processes *Glob. Mon. Weather Rev.* **134** 2318–41

Hou X *et al* 2019 Impacts of transboundary air pollution and local emissions on $PM_{2.5}$ pollution in the Pearl River Delta region of China and the public health, and the policy implications *Environ. Res. Lett.* **14** 034005

Huang R J *et al* 2014 High secondary aerosol contribution to particulate pollution during haze events in China *Nature* **514** 218–22

Huang X *et al* 2020 Enhanced secondary pollution offset reduction of primary emissions during COVID-19 lockdown in China *Natl Sci. Rev.* **8** nwaa137

Kang Y *et al* 2016 High-resolution ammonia emissions inventories in China from 1980 to 2012 *Atmos. Chem. Phys.* **16** 2043–58

Kusaka H *et al* 2001 A simple single-layer urban canopy model for atmospheric models: comparison with multi-layer and slab models *Bound.-Layer Meteorol.* **101** 329–58

Li M *et al* 2014 Haze in China: current and future challenges *Environ. Pollut.* **189** 85–86

Li M *et al* 2017 MIX: a mosaic Asian anthropogenic emission inventory under the international collaboration framework of the MICS-Asia and HTAP *Atmos. Chem. Phys.* **17** 935–63

Liu F *et al* 2016 Recent reduction in NO_x emissions over China: synthesis of satellite observations and emission inventories *Environ. Res. Lett.* **11** 114002

Ministry of Ecology and Environment of the People's Republic of China (MEE) 2016 *Report on the State of the Environment in China 2013* (available at: http://english.mee.gov.cn/Resources/Reports/soe/soe2011/201606/P020160601591756378883.pdf) (Accessed: 29 September 2020)

Ministry of Ecology and Environment of the People's Republic of China (MEE) 2018 *Report on the State of the Ecology and Environment in China 2017* (available at: http://english.mee.gov.cn/Resources/Reports/soe/SOEE2017/201808/P020180801597738742758.pdf) (Accessed: 29 September 2020)

Mlawer E J *et al* 1997 Radiative transfer for inhomogeneous atmospheres: RRTM, a validated correlated-k model for the longwave *J. Geophys. Res.-Atmos.* **102** 16663–82

Morrison H *et al* 2009 Impact of cloud microphysics on the development of trailing stratiform precipitation in a simulated squall line: comparison of one- and two-moment schemes *Mon. Weather Rev.* **137** 991–1007

Pan Y *et al* 2018 Identifying ammonia hotspots in China using a national observation network *Environ. Sci. Technol.* **52** 3926–34

Pinder R W *et al* 2006 Temporally resolved ammonia emission inventories: current estimates, evaluation tools, and measurement needs *J. Geophys. Res.-Atmos.* **111** D16310

Seinfeld J H and Pandis S N 2006 *Atmospheric Chemistry and Physics: From Air Pollution to Climate Change* (New York: Wiley)

Song S *et al* 2018 Fine-particle pH for Beijing winter haze as inferred from different thermodynamic equilibrium models *Atmos. Chem. Phys.* **18** 7423–38

Song S *et al* 2019 Thermodynamic modeling suggests declines in water uptake and acidity of inorganic aerosols in Beijing winter haze events during 2014/2015–2018/2019 *Environ. Sci. Technol. Lett.* **6** 752–60

State Council of the People's Republic of China (SC) 2013 *Notice of the State Council on Issuing the Action Plan on Prevention and Control of Air Pollution* (available at: www.gov.cn/zhengce/content/2013-09/13/content_4561.htm) (Accessed: 29 September 2020)

State Council of the People's Republic of China (SC) 2018 *Notice of the State Council on Issuing the Three-year Action Plan Fighting for a Blue Sky* (available at: www.gov.cn/zhengce/content/2018-07/03/content_5303158.htm) (Accessed: 29 September 2020)

Sun Y *et al* 2012 Characterization of summer organic and inorganic aerosols in Beijing, China with an aerosol chemical speciation monitor *Atmos. Environ.* **51** 250–9

Sun Y *et al* 2016 Rapid formation and evolution of an extreme haze episode in Northern China during winter 2015 *Sci. Rep.* **6** 27151

Van Damme M *et al* 2014 Global distributions, time series and error characterization of atmospheric ammonia (NH_3) from IASI satellite observations *Atmos. Chem. Phys.* **14** 2905–22

Wang Y *et al* 2013 Sulfate-nitrate-ammonium aerosols over China: response to 2000–2015 emission changes of sulfur dioxide, nitrogen oxides, and ammonia *Atmos. Chem. Phys.* **13** 2635–52

Wiedinmyer C *et al* 2011 The Fire INventory from NCAR (FINN): a high resolution global model to estimate the emissions from open burning *Geosci. Model Dev.* **4** 625–41

Xu Z *et al* 2019 High efficiency of livestock ammonia emission controls in alleviating particulate nitrate during a severe winter haze episode in northern China *Atmos. Chem. Phys.* **19** 5605–13

Zaveri R A *et al* 2008 Model for Simulating Aerosol Interactions and Chemistry (MOSAIC) *J. Geophys. Res.* **113** D13204

Zaveri R A and Peters L K 1999 A new lumped structure photochemical mechanism for large-scale applications *J. Geophys. Res.-Atmos.* **104** 30387–415

Zhang L *et al* 2012 Nitrogen deposition to the United States: distribution, sources, and processes *Atmos. Chem. Phys.* **12** 4539–54

Zhang L *et al* 2015 Source attribution of particulate matter pollution over North China with the adjoint method *Environ. Res. Lett.* **10** 084011

Zhang L *et al* 2018 Agricultural ammonia emissions in China: reconciling bottom-up and top-down estimates *Atmos. Chem. Phys.* **18** 339–55

Zhang Q *et al* 2019a Drivers of improved $PM_{2.5}$ air quality in China from 2013 to 2017 *Proc. Natl Acad. Sci. USA* **116** 24463–9

Zhang Q *et al* 2019b Bias in ammonia emission inventory and implications on emission control of nitrogen oxides over North China Plain *Atmos. Environ.* **214** 116869

Zhao P S *et al* 2013 Characteristics of concentrations and chemical compositions for $PM_{2.5}$ in the region of Beijing, Tianjin, and Hebei, China *Atmos. Chem. Phys.* **13** 4631–44

Zheng B *et al* 2018 Trends in China's anthropogenic emissions since 2010 as the consequence of clean air actions *Atmos. Chem. Phys.* **18** 14095–111

Zheng G *et al* 2020 Multiphase buffer theory explains contrasts in atmospheric aerosol acidity *Science* **369** 1374–7

Zhu L *et al* 2015 Global evaluation of ammonia bidirectional exchange and livestock diurnal variation schemes *Atmos. Chem. Phys.* **15** 12823–43